Applied Catalysis A: General 443–444 (2012) 103–110

Contents lists available at SciVerse ScienceDirect

Applied Catalysis A: General

journal homepage: www.elsevier.com/locate/apcata

Liquid-phase alkylation of benzene with ethylene over postsynthesized MCM-56 analogues

Bin Zhang[a,b], Yongjun Ji[a], Zhendong Wang[a], Yueming Liu[a], Hongmin Sun[b], Weimin Yang[b], Peng Wu[a,*]

[a] Shanghai Key Laboratory of Green Chemistry and Chemical Processes, Department of Chemistry, East China Normal University, North Zhongshan Rd. 3663, Shanghai 200062, PR China

[b] Shanghai Research Institute of Petrochemical Technology, SINOPEC, North Pudong Rd. 1658, Shanghai 201208, PR China

ARTICLE INFO

Article history:
Received 1 March 2012
Received in revised form 21 July 2012
Accepted 23 July 2012
Available online 28 July 2012

Keywords:
MCM-56 analogue
MCM-22
Postsynthesis
Liquid-phase alkylation
Ethylbenzene

ABSTRACT

MCM-56 analogues were postsynthesized via a mild acid treatment technique from hydrothermally synthesized MCM-22 lamellar precursors with Si/Al ratios of 15–45. The physicochemical properties of MCM-56 were characterized by XRD, SEM, N_2 adsorption, XPS, ^{29}Si and ^{27}Al MAS NMR, NH_3-TPD and pyridine adsorption IR techniques. In comparison to MCM-22 with 3-dimensional MWW topology, the postsynthesized MCM-56 showed a broad X-ray diffraction of emerged 1 0 1 and 1 0 2 reflections and possessed a structural disorder along the layer stacking direction. Composed of partially delaminated MWW nanosheets, MCM-56 analogues had a larger external surface than MCM-22. The MCM-56 and MCM-22 catalysts were employed in the liquid-phase alkylation of benzene with ethylene. MCM-56 analogues exhibited a higher yield of ethylated benzenes and a higher catalytic stability than MCM-22, proving to serve as promising solid-acid catalysts for processing bulky molecules in petrochemical industry.

1. Introduction

Alkylation of benzene is an important process in petrochemical industry [1–3]. As one of the most useful alkylbenzenes, ethylbenzene (EB) is used as feedstock for the production of styrene, the raw material for polystyrene, acrylonitrile–butadiene–styrene (ABS), styrene–acrylonitrile (SAN) resins, styrene–butadiene elastomers and latexes, as well as other unsaturated resins [4]. The worldwide capacity of ethylbenzene currently reaches 35 million metric tons per year. Its global demand is estimated to grow by about 4.1% annually in the period of 2009–2014 and by 3.3% per year over the ten years of the forecast.

Nowadays, ethylbenzene is mainly produced by the alkylation of benzene with ethylene or ethanol using acid catalysts [5]. The conventional catalysts for this reaction are mineral acids such as aluminum chloride and phosphoric acid. These homogeneous catalysts cause a number of problems in terms of handling, safety, corrosion, and waste disposal in spite of their relatively high activity and long lifetime [6–8]. An immense endeavor has been put to develop alternative catalytic systems that are more environmentally friendly. As a result, the ethylbenzene production technology has progressively shifted to zeolite-based processes [9]. Using ZSM-5 based catalyst [10,11], the process of ethylbenzene production under gas-phase conditions was first commercialized by Mobil/Badger. Thereafter, a series of zeolites were investigated to exhibit promising catalytic performances. USY [7,12], Beta [13,14] and MCM-22 [15,16] have been successively commercialized for the liquid-phase alkylation of benzene which is operated at low temperatures and high pressures with the advantage of a better control and a longer catalyst life. With respect to the ethylbenzene production with USY, Beta or MCM-22 as the catalyst, MCM-22 possesses a higher selective for ethylated benzenes at a lower benzene/ethylene molar ratio, which is benefit for reducing the recycling amount of benzene [17].

MCM-22 zeolite with the MWW topology [18], one of the most representative zeolite developed by Mobil [19], is structurally analogous to SSZ-25 [20], PSH-3 [21], ITQ-1 [22] and MCM-49 [23]. Originated from a lamellar precursor, the MCM-22 structure is composed of three pore systems. One is the 2-dimensional (2D) sinusoidal 10-membered ring (MR) channel with elliptical ring cross section of 0.45 nm × 0.55 nm, which runs through the intralayers of the MWW nanosheets. The other interlayer 10-MR channel contains 12-MR supercages of 0.71 nm × 0.71 nm × 1.82 nm. It has also 12-MR side pockets or half cups on the outer crystallite surfaces external, providing more accessible acid sites for catalytic reactions.

As an important member of MWW family, MCM-56 has been paid more attention because its side pockets on the external surface are easily accessible by large molecules [24]. Consisting of disordered collection of MWW sheets but more exposed side pockets, MCM-56 is claimed to possess a partially delaminated structure in

* Corresponding author. Fax: +86 21 62232292.
E-mail address: pwu@chem.ecnu.edu.cn (P. Wu).

0926-860X/$ – see front matter © 2012 Elsevier B.V. All rights reserved.
http://dx.doi.org/10.1016/j.apcata.2012.07.028

comparison to 3D crystalline MCM-22. MCM-56 was once prepared only by hydrothermal synthesis from the synthetic gels similar to MCM-22. The hydrothermal synthesis of MCM-56 usually needs a more careful control for crystallization time and temperature in comparison to the synthesis of MCM-22. Furthermore, the variation of the Si/Al ratios is limited in the direct hydrothermal synthesis of MCM-56 [25].

Recently, we developed a facial postsynthesis method for preparing MCM-56 analogues MWW-type aluminosilicate or titanosilicate precursors with changeable Al or Ti content [26,27], which is based on the fact that 2D lamellar precursors are of soft materials with a structural diversity. In comparison to corresponding 3D MWW counterparts, the obtained MCM-56 analogues exhibit enhanced catalytic activity in the reactions such as alkene epoxidation and 1,3,5-triisopropyl benzene cracking.

With the purpose to develop more active and selective catalysts than 3D MCM-22 for the alkylation of benzene, we postsynthesized MCM-56 analogues having a wide range of Si/Al ratios through a mild acid treatment in this study. The resulting materials were characterized for the structural features and physicochemical properties in detail. Their catalytic performance was investigated in the liquid-phase alkylation of benzene with ethylene.

2. Experimental

2.1. Synthesis MCM-22 precursors and H-MCM-22 samples

MCM-22 lamellar precursors were hydrothermally synthesized using hexamethyleneimine (HMI) as a structure-directing agent (SDA) following the literature reported previously [9]. Silica gel (40 wt.%) and $Al_2(SO_4)_3{\cdot}18H_2O$ were used as silicon and aluminum sources, respectively. The precursors were crystallized from the gels with molar compositions of 1.0 SiO_2:1/n Al_2O_3:0.10 NaOH:0.45 HMI:20.0 H_2O, where n was 30, 40, 60 and 90. The crystallization was carried out in Teflon-lined stainless autoclaves under rotation (200 rpm) at 423 K for 4 days. The precipitates were filtered, washed with deionized water and dried at 373 K overnight. The as-synthesized precursors, denoted as MCM-22(P), were calcined in air at 723 K for 5 h to remove the organic SDA species. Calcined MCM-22 in sodium-form was ion exchanged with 1 M NH_4NO_3 at room temperature for 6 h twice and then calcined at 723 K for 5 h to obtain the proton-type sample, H-MCM-22.

2.2. Postsynthesis of MCM-56 analogues

MCM-56 analogues were prepared from MCM-22(P) by postsynthesis method that we reported elsewhere [27]. Under mild acid treatment conditions, MCM-22(P) was structurally transferred to MCM-56 readily. In a typical preparation, MCM-22(P) was treated with 0.1 M HNO_3 at a solid-to-liquid weight ratio of 1:20 and room temperature for 1 h. The acid treated samples were subsequently calcined and changed into proton-type MCM-56 using the same procedures mentioned above for H-MCM-22.

2.3. Characterization methods

The crystallinity of the samples was characterized by X-ray powder diffraction (XRD) patterns on a Bruker D8 Advance diffractometer equipped with a rotating anode and Cu-Kα radiation (λ = 1.5405 Å). Scanning electron microscopy (SEM) was performed on a Hitachi S-4800 electron microscope. N_2 adsorption was carried out at 77 K on a BELSORP-MAX instrument. The samples were degassed under vacuum at 383 K for 4 h and then at 623 K for 6 h. Fourier transform infrared spectra (FTIR) were obtained with a Nicolet FTIR-380 spectrometer at room pressure. A self-supported wafer (50 mg and Ø 2 cm) was set in a quartz IR cell sealed with CaF_2 windows, where it was evacuated at 773 K for 2 h before the pyridine adsorption. The adsorption was carried out by exposing the wafer to a pyridine vapor (1.3 kPa) at room temperature for 0.5 h. The IR spectra of chemically adsorbed pyridine were recorded after evacuation at 473 K, 573 K or 673 K for 1 h. The acid-site distribution was measured with NH_3 temperature programmed desorption (NH_3-TPD) on an apparatus equipped with a thermal conductivity detector (TCD). A sample of 150 mg was activated in helium flow at 873 K for 1 h. It was then cooled to 373 K where adsorption of NH_3 and desorption physically adsorbed NH_3 were preformed. The NH_3-TPD profile was recorded by heating the sample from 373 K to 873 K at a rate of 10 K min^{-1} and under helium flow at the rate of 30 cm^3 min^{-1}. Solid-state MAS NMR spectra were recorded on a Bruker DMX Advance 500 spectrometer. ^{29}Si NMR spectra were recorded at 59.62 MHz with a pulse length of 5 μs and a spinning rate of 4 kHz, while ^{27}Al NMR spectra were recorded at 78.20 MHz with a pulse length of 0.31 μs and a spinning rate of 12 kHz. Si/Al molar ratios were determined by inductively coupled plasma (ICP) elemental analyses on a Varian 725-ES optical emission spectrometer. X-ray photoelectron spectroscopy (XPS) measurements were performed on ESCALAB 250 (VG) using Al Kα ($h\nu$ = 1486.6 eV) radiation.

2.4. Catalytic reactions

The prepared catalysts, MCM-22 and MCM-56 analogues, were pressed into self-supported tablets under 20 MPa pressure using an electric tablet machine. They were then scrapped to collect the granules with a griddle of 10–20 mesh. The shaped tablets were tested for liquid-phase alkylation of benzene with ethylene in a fixed bed reactor. The catalyst (1 g) was loaded into the middle of the stainless reactor (L = 750 mm, D = 10 mm), and it was activated at 673 K under nitrogen flow to eliminate any adsorbed water. The reactor was then brought to the reaction temperature of 463 K where the alkylation was operated continuously at 3.0 MPa, benzene to ethylene molar ratio of 3.0 and weight hourly space velocity (WHSV) of 1.0 or 2.0 h^{-1} for ethylene. The reaction products were collected and analyzed with an Agilent 6820 gas chromatograph equipped with a flame ionization (FID) detector and a HP-FFAP (50 m × 0.32 mm × 0.25 μm) capillary column. In poisoning experiments, 2,4-dimethylquinoline (DMQ), employed as a poisonous substance, was co-fed into the reactor continuously at a rate of 50 μL h^{-1} by mixing in benzene.

3. Results and discussion

3.1. Postsynthesis of MCM-56 analogues with various Si/Al ratios

The MCM-22(P) precursors were synthesized at various Si/Al ratios (15, 20, 30 and 45) using HMI as SDA. The XRD patterns of these precursors before and after acid treatment with 0.1 M HNO_3 are given in Fig. 1. The precursors all showed the 0 0 1 and 0 0 2 diffraction peaks in the 2θ region of 3–7°, characteristic of a layered structure with the MWW sheets stacking along the c-direction (Fig. 1A). In addition, the MCM-22(P) samples also showed three well resolved diffractions due to 1 0 0, 1 0 1 and 1 0 2 planes. The diffractions related to the crystalline MWW sheets parallel to the ab-planes such as 3 1 0 plane were also clearly observed in higher angle region. The XRD patterns matched well with that of the MWW lamellar precursor reported in the literature [18,28]. Thus, the materials with a pure MWW phase were obtained at different Si/Al ratios. Fig. 1B shows the XRD patterns of directly calcined MCM-22 precursors. They were obviously different from those of corresponding precursors. Upon calcination, the 0 0 1 and 0 0 2 diffractions shifted to higher angles with reduced intensities,

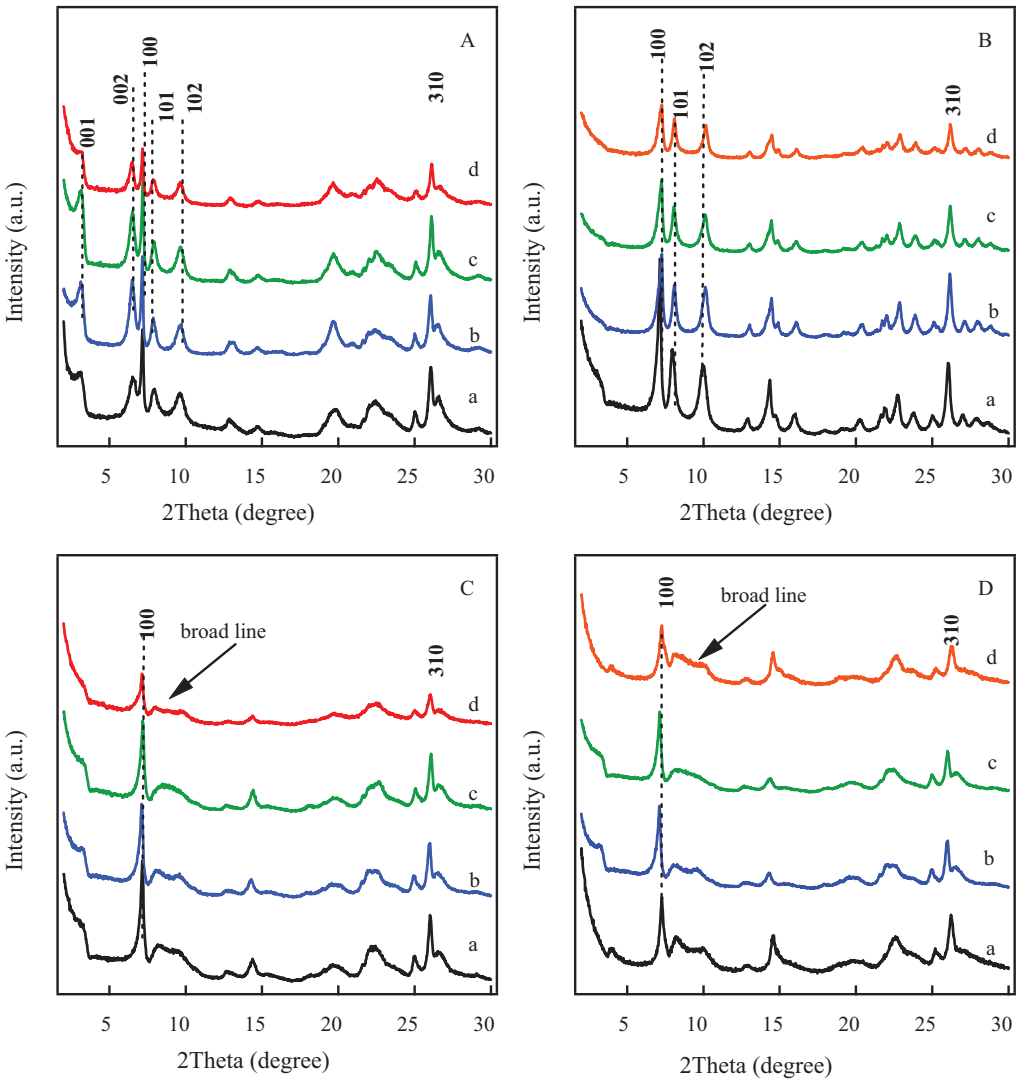

Fig. 1. XRD patterns of MCM-22 precursors (A), directly calcined MCM-22 precursors at 823 K (B), MCM-56 analogues as-made from the MCM-22 precursors by treatment in 0.1 M HNO_3 for 0.5 h (C), and calcined MCM-56 analogues at 823 K (D). The samples were hydrothermally synthesized at Si/Al ratio of 15 (a), 20 (b), 30 (c) and 45 (d), respectively.

and were almost invisible in the patterns. On the other hand, the *h k* 0 diffractions such as 1 0 0 and 3 1 0 peaks remained practically unchanged, indicating that the structural change took place essentially along the *c*-axis. It means that 2-dimensional (2D) lamellar precursors were transformed into 3D MWW structure as a result of interlayer dehydration/condensation of the hydroxyl groups on the layers upon calcination.

However, the MCM-22(P) samples were converted to the products which showed MCM-56-like XRD patterns after a mild acid treatment in 0.1 M HNO_3 at room temperature (Fig. 1C). The line positions and relative intensities of the peaks were in good agreement with those reported for directly synthesized MCM-56 aluminosilicates [24]. They were featured by a very broad diffraction in the 2θ region of 7–11°, since the 1 0 1 and 1 0 2 diffractions overlapped seriously. Nevertheless, the *ab*-plane-related diffractions parallel to such as 1 0 0 and 3 1 0 peaks remained well-resolved. To distinguish the reported MCM-56 aluminosilicates that were hydrothermally synthesized under controlled conditions, we denote the present postsynthesized materials as MCM-56 analogues. It seems that the acid treatment kept the MWW sheets almost intact but caused a structural change only in their arrangement and stacking format. The broad band in the 2θ region of 7–11° could be taken as a clear evidence for the formation of a structure analogue to MCM-56 [29]. Fig. 1D showed the XRD patterns of the MCM-56 analogues calcined at 723 K for 5 h. The patterns remained the same in terms of the overlapped 1 0 1 and 1 0 2 diffractions, which indicates that the structure of MCM-56 analogues was thermally stable.

We once reported that a mild acid treatment may extract partially the organic SDA molecules intercalated between the MWW layers, leading to an unbalanced array or stacking of the layers [27,29]. After further calcination, the interlayer condensation then takes place in a way which is different from an ordinary manner in direct calcination of the precursor. Fig. 2 summarizes possible formation mechanism of postsynthesized MCM-56 analogues. The disordered collection of MWW layers may make more edges of the structure expose to the outside, thus MCM-56 is claimed to possess a partially delaminated structure [30]. As a result, the MCM-56 analogues were prepared successfully by postsynthesis from the corresponding MCM-22 precursors. In direct synthesis, the formation of MCM-56 structure is needed to optimize the crystallization degree and gel compositions [25]. However, by

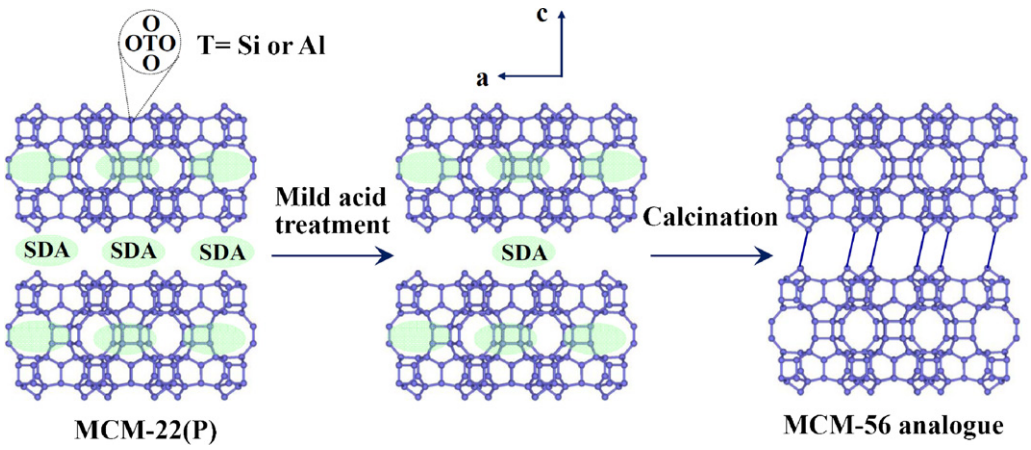

Fig. 2. Strategy for post-synthesizing MCM-56 analogue.

using present postsynthesis technique with a mild acid treatment, the structure of MCM-56 analogues was constructed readily from fully crystallized precursors independent of Si/Al ratio.

3.2. Physicochemical properties of MCM-56 analogues

The scanning electron micrograph (SEM) images of MCM-22 and MCM-56 analogue are shown in Fig. S1 in Supplementary information. MCM-22 was composed of thin pellet-like crystallites, approximately 0.02–0.05 μm in thickness and 0.2–0.5 μm in length. The SEM image of MCM-56 analogue indicated that its crystallites also appeared to be thin platelets with the same crystal size as MWW-22. The HNO_3 treatment and subsequent calcination had no significant influence on the crystallite morphology, although the XRD patterns clearly evidenced a structural transformation occurred along the *c*-axis. The acid treatment-induced structure change probably occurred at a nanometer or subnanometer scale but not at a micrometer level.

The physicochemical properties of MCM-22 and MCM-56 analogue were characterized by various techniques (Table 1). They were both obtained from the same precursor synthesized at Si/Al ratio of 15. The XPS and ICP analyses indicated that the Si/Al molar ratio on the crystallite surface of MCM-22 was equal to the bulk ratio determined, suggesting the Al distribution was relatively uniform throughout the crystallites. On the other hand, the Si/Al molar ratio of MCM-56 analogue increased from 15.8 in the bulk phase to 17.9 on the surface, indicating a slight dealumination took place during acid treatment especially on the crystallite surface. This phenomenon was in accordance with that reported in previous literature [27]. In comparison with MCM-22, MCM-56 analogue showed a slightly lower N_2 adsorption amount in the isotherm at P/P_0 = 0–0.75, but a higher amount in higher P/P_0 region (see Fig. S2 in Supplementary information), verifying that MCM-56 possessed a more exposed external surface [28]. According to analysis using *t*-plot method [31], the external surface area of MCM-56 analogue was 145 $m^2\,g^{-1}$, which was larger than that of MCM-22 (118 $m^2\,g^{-1}$). This was in agreement with the results reported on hydrothermally synthesized MCM-56 which was assumed to be composed of the MWW sheets arrayed in a disordered manner and have so-called partially delaminated structure [25,28].

Table 1
A comparison of physicochemical properties between H-MCM-22 and H-MCM-56 analogue.

Sample	Bulk Si/Al[a]	Surface Si/Al[b]	$V_{micropore}$ [c] ($cm^3\,g^{-1}$)	Specific surface area ($m^2\,g^{-1}$)		
				S_{total} [d]	$S_{micropore}$ [c]	$S_{external}$ [e]
H-MCM-22	15.5	15.7	0.17	476	358	118
H-MCM-56	15.8	17.9	0.14	415	270	145

[a] Given by ICP.
[b] Given by XPS.
[c] Micropore volume and surface area were calculated by *t*-plot method.
[d] Calculated by BET method.
[e] $S_{external} = S_{total} - S_{micropore}$.

^{29}Si spectroscopy was used to investigate the development of external silanols (Fig. 3A). All the bands matched well with those previously reported for MCM-22 [32–34]. H-MCM-56 showed a more intensive resonance around −100 ppm which was assigned to the Q^3 sites such as $Si(OH)(SiO)_3$ and $Si(OAl)(SiO)_3$ [28]. Since the acid treatment caused a partial dealumination during the postsynthesis of H-MCM-56, the −100 ppm resonance was considered to originate mainly from the $Si(OH)(SiO)_3$ groups. ^{27}Al MAS NMR spectra of H-MCM-22 and H-MCM-56 both showed clearly two sets of signals, that is, a broader band with a maximum at 55 ppm and a low frequency signal around 0 ppm (Fig. 3B), which are assigned to tetrahedral and octahedral Al species, respectively [35].

IR spectra were measured to investigate the characters of hydroxyl groups and acid sites in H-MCM-22 and H-MCM-56 analogue. The bands at 3745 cm^{-1} and 3620 cm^{-1} are attributed to the external isolated silanols and the structure Si(OH)Al hydroxyls associated with framework Al, respectively [36]. MCM-56 analogue showed a more intensive band at 3745 cm^{-1} than that of MCM-22 (see Fig. S3 in Supplementary information), which is probably related to a large portion of MWW sheets exposed on the external surface. The reduced intensity of the 3620 cm^{-1} band in MCM-56 analogue is partially due to the framework dealumination by acid treatment. A disordered collection of MWW sheets may also cause a part of structural hydroxyl groups decrease. The pyridine adsorption and desorption spectra were further taken to measure the acidic properties of H-MCM-22 and H-MCM-56. The desorption of pyridine was performed at different temperatures (473–673 K) to give information about the strength of acid sites. The band at 1545 cm^{-1} due to pyridinium ion could be taken as the evidence of Brønsted acid sites, whereas the band at 1450 cm^{-1} due to coordinated pyridine corresponds to Lewis acid sites [36]. And the pyridine molecules adsorbed on these two kinds of acid sites both contribute to the band at 1490 cm^{-1}. The spectra of H-MCM-22 and H-MCM-56 analogue were both dominated by the 1545 cm^{-1} band (Fig. 4), indicating they were characteristic of Brønsted acidity. In comparison to H-MCM-22, H-MCM-56 showed slightly decreased intensity at 1545 cm^{-1} band, which might be caused by the disordered stacking of MWW sheets. After desorption at 673 K, the 1450 cm^{-1} band was still observed and showed relatively a high

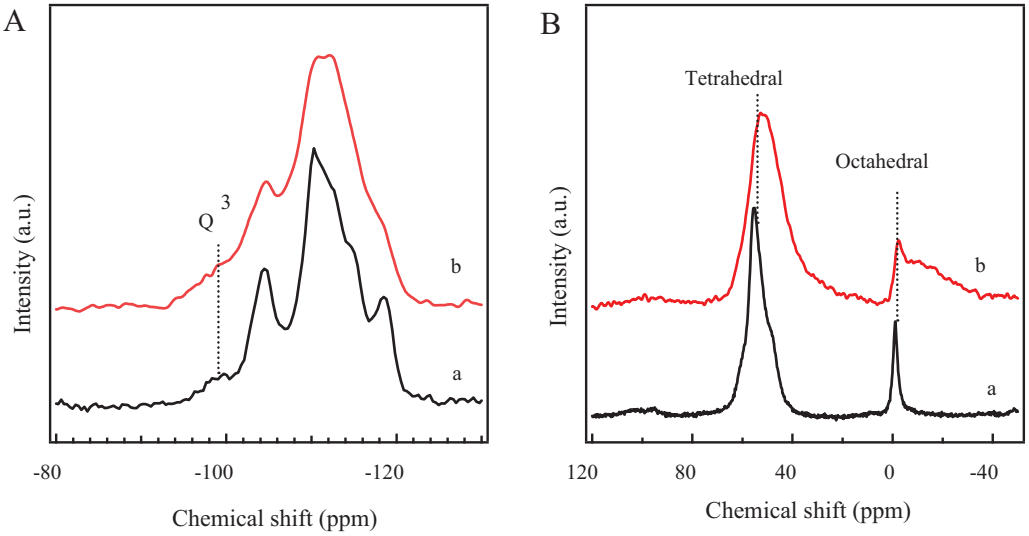

Fig. 3. ^{29}Si (A) and ^{27}Al (B) MAS NMR spectra of H-MCM-22 (a) and H-MCM-56 (b).

intensity (see Table S1 in Supplementary information), implying the zeolites contained strong acid sites.

NH_3-TPD profiles of H-MCM-22 and H-MCM-56 analogue are shown in Fig. S4 in Supplementary information. They exhibited desorption peaks typically characteristic of MCM-22 zeolite [37,38]. The peak around 487 K corresponded to the desorption of ammonia adsorbed on weak acid sites, whereas the peak at 668 K was assigned to the desorption of ammonia adsorbed on strong acid sites. In agreement with above IR spectra of pyridine adsorption, the amount of acidic sites in H-MCM-56 decreased slightly in comparison to H-MCM-22. Nevertheless, showing the ammonia desorption peaks at the same temperatures, these two zeolites were comparable in the strength of acid sites.

3.3. Catalytic properties of H-MCM-56 analogues in alkylation of benzene with ethylene

Hydrothermally synthesized MCM-56 is reported to show unique catalytic performance as a solid-acid catalyst which was similar or even superior to other zeolites such as ZSM-5, Beta and MCM-22 in particular reactions such as benzene alkylation [24,30] and as an adsorbent for separation processes [39,40]. In comparison to MCM-22, the advantage of MCM-56 in production of isopropylbenzene is closely related to its open external surface which makes the active sites more accessible to the reactant molecules [41]. The successful postsynthesis of MCM-56 encouraged us to investigate its catalytic behaviors in the reactions involving bulky substrates.

As an important reaction for producing ethylbenzene, the alkylation of benzene with ethylene is currently catalyzed by solid-acid catalysts of zeolites, that is, H-ZSM-5 catalyst in gas-phase reactions and H-Beta or H-MCM-22 in liquid-phase reactions. This reaction is comprised of complicated processes, which includes the alkylation of benzene with ethylene to ethylbenzene, further alkylation of ethylbenzene to diethylbenzenes or poly ethylbenzenes [13], isomerization of ethylbenzene, oligomerization of ethylene [42] and generation of other aromatic hydrocarbons [43]. Table 2 compares the catalytic activity and product distribution between H-MCM-22 and H-MCM-56 analogue in liquid-phase alkylation of benzene with ethylene operated continuously at 3.0 MPa and 463 K. The reaction products were made up of ethylbenzene (EB), xylenes (Xys), *para*-diethylbenzene (*p*-DEB), *ortho*-diethylbenzene (*o*-DEB), *meta*-diethylbenzene (*m*-DEB), triethylbenzenes (TEB), C_9–C_{11} and other by-products. As shown in Fig. 5, the yield of ethylated benzenes (EBs, including EB, DEB and TEB) varied with the reaction

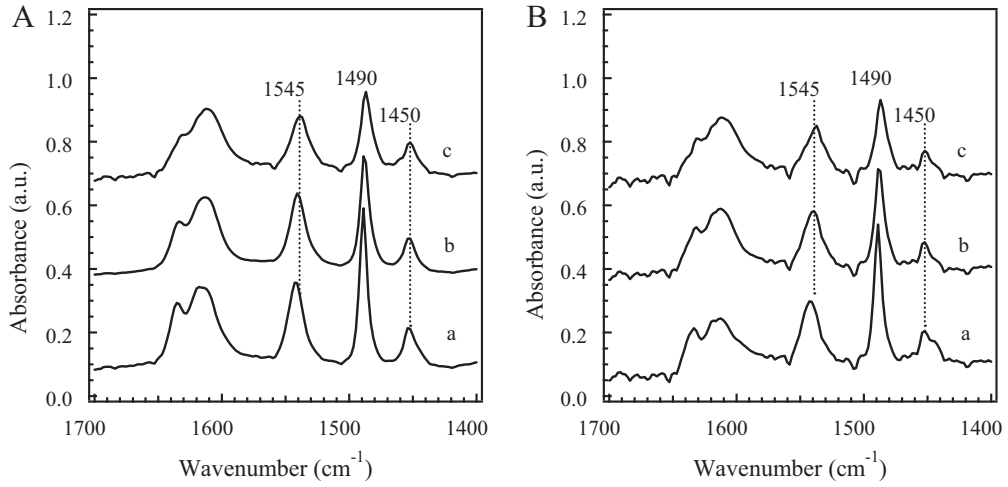

Fig. 4. IR spectra of H-MCM-22 (A) and H-MCM-56 (B) after pyridine adsorption and then desorption at 473 K (a), 573 K (b) and 673 K (c) for 1 h, respectively.

Table 2
Catalytic activity and product distribution in the liquid-phase alkylation of benzene with ethylene on H-MCM-22 and H-MCM-56 analogue.[a]

Catalyst[b]	Benzene conv. (%)	Product distribution (%)							
		EB	*m*-DEB	*p*-DEB	*o*-DEB	TEB	Xys	C_9–C_{11}	Others
H-MCM-22	27.7	81.6	4.3	3.9	6.5	1.4	0	0.3	2.0
H-MCM-56	32.9	82.6	4.2	3.5	6.5	1.5	0	0.2	1.5

[a] Reaction conditions: catalyst, 1.0 g; temperature, 463 K; pressure, 3.0 MPa; benzene/ethylene molar ratio, 3.0; ethylene WHSV, 1.0 h^{-1}; TOS = 20 h.
[b] The zeolite catalysts were prepared from the same precursor, MCM-22-P(15).

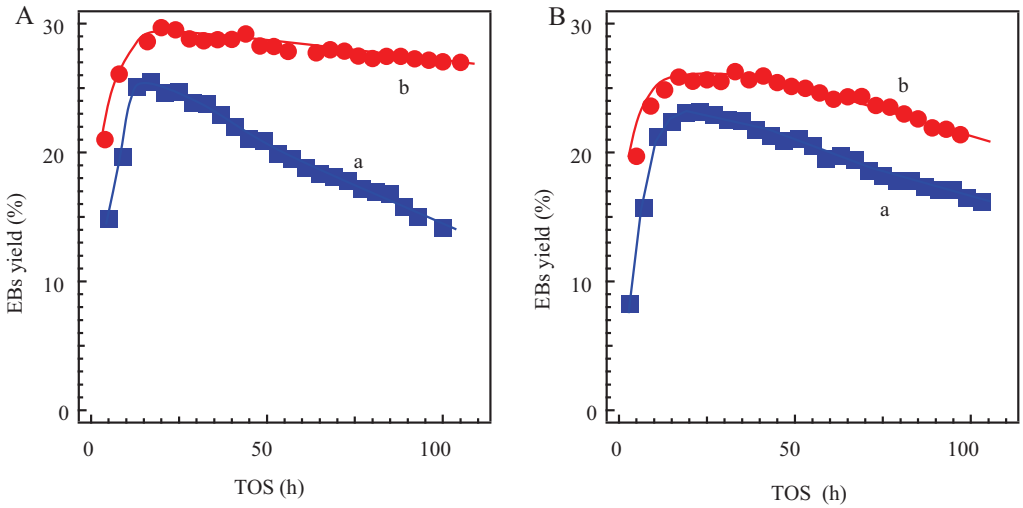

Fig. 5. A comparison of catalytic performance between H-MCM-22 (a) and H-MCM-56 (b) with different Si/Al ratios. The samples were prepared from MCM-22-P(15) (A) and MCM-22-P(20) (B), respectively. Reaction conditions: catalyst, 1.0 g; temperature, 463 K; pressure, 3.0 MPa; benzene/ethylene molar ratio, 3.0; ethylene WHSV, 2.0 h^{-1}.

time on different WHSV of ethylene. A reasonable comparison is thus made by using the results obtained at time on stream (TOS) of 20 h, where both MCM-22 and MCM-56 gave the highest activity. Obtained from the same MCM-22 precursor (Si/Al = 15), the H-MCM-56 analogue showed an enhanced benzene conversion and ethylbenzene selectivity in comparison to H-MCM-22 counterpart (Table 2). Moreover, the operating conditions play an important role in catalytic performances and duration. For liquid-phase alkylation of benzene with ethylene, a high WHSV of ethylene is beneficial for increasing the production capacity of alkylbenzenes, which is however accompanied by a quicker deactivation of the catalyst (see Fig. S5 in Supplementary information). Herein, the reactions were carried out either at ethylene WHSV of 1.0 h^{-1} or 2.0 h^{-1} depending on different purpose.

In commercial process for ethylbenzene production, diethylbenzenes and triethylbenzenes are also regarded as objective products in addition to ethylbenzene because they are finally converted into high valuable and desirable ethylbenzene product through catalytic transalkylation with benzene. Thus, the sum of mono- and poly-ethylbenzenes is employed to evaluate the catalyst performance in benzene ethylation. The dependence of ethylated benzenes (EBs, including EB, DEB and TEB) and EBs selectivity on the Al content in H-MCM-22 and H-MCM-56 is presented in Fig. 6. The catalysts were prepared from the MCM-22 precursors with

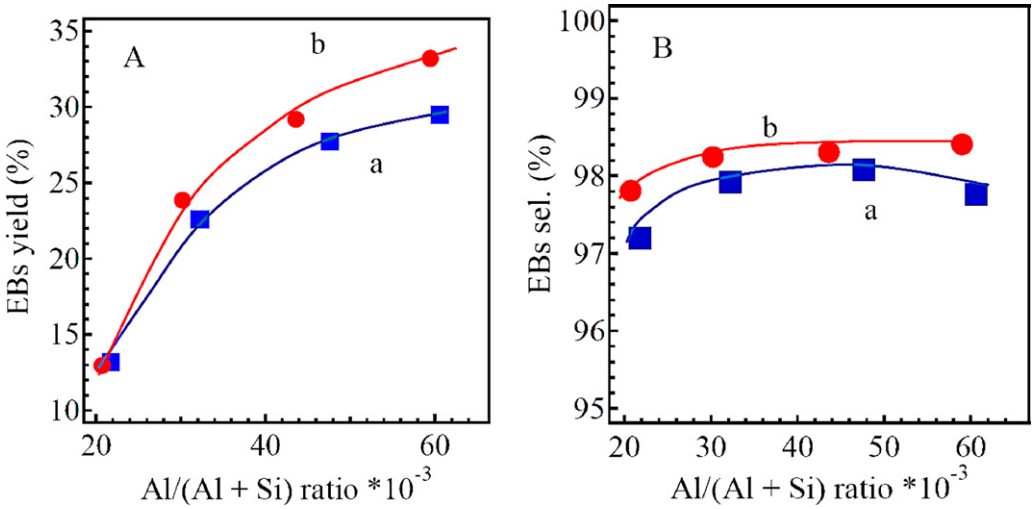

Fig. 6. Dependence of ethylated benzenes (EBs) (A) and EBs selectivity (B) on the Al content in H-MCM-22 (a) and H-MCM-56 (b). Reaction conditions: catalyst, 1.0 g; temperature, 463 K; pressure, 3.0 MPa; benzene/ethylene molar ratio, 3.0; ethylene WHSV, 1.0 h^{-1}; TOS = 20 h.

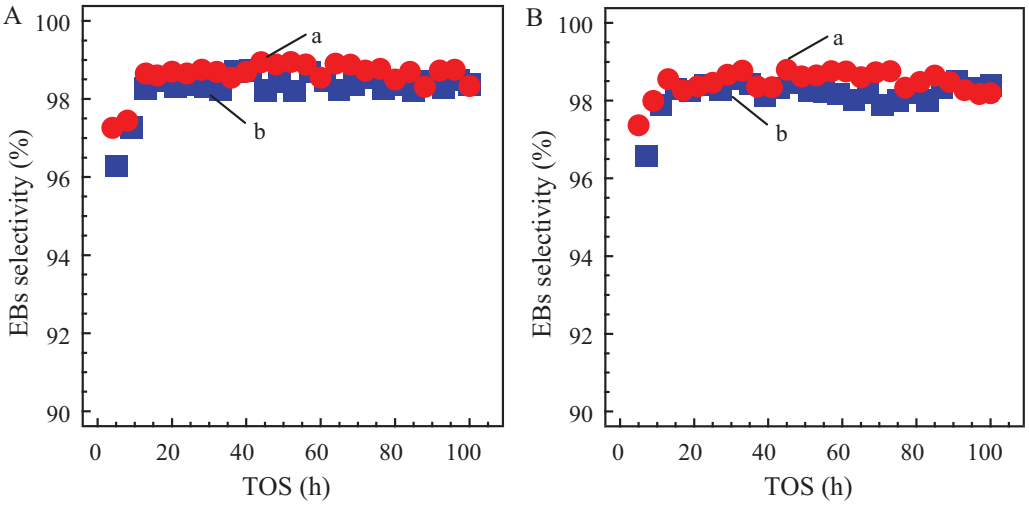

Fig. 7. A comparison of EBs selectivity between H-MCM-22 (a) and H-MCM-56 (b). The samples were prepared from MCM-22-P(15) (A) and MCM-22-P(20) (B), respectively. Reaction conditions: see Fig. 6.

Si/Al molar ratios of 15, 20, 30 and 40. An obvious improvement in EBs yield was achieved by post-converting the precursors into H-MCM-56 analogues especially in the region of high Al content. The increase of EBs yield became less with deceasing Al content, i.e. increasing Si/Al ratio. Meanwhile, the EBs selectivity in total products was also enhanced to a certain degree by post-synthesizing MCM-56 analogues (Fig. 6B).

In order to investigate whether MCM-56 analogue was superior to MCM-22 in duration and lifetime, the reaction was carried out at an increased WHSV of ethylene (2.0 h^{-1}) and the reaction time was prolonged to 100 h of TOS. As shown in Fig. 5, two sets of catalysts prepared form the precursors with Si/Al molar ratios of 15 and 20 were compared. Generally, the reactions took about 15 h to reach the highest catalytic activity. MCM-56 showed almost a stable reaction level at TOS of 20–75 h, while MCM-22 deactivated more rapidly after 20 h. The EBs selectivity was always maintained around 98% independent of reaction time (Fig. 7). H-MCM-56 not only showed higher EBs yield and but also exhibited to be more durable than H-MCM-22 especially in the sample at Si/Al molar ratio of 15 (Fig. 5A). The EBs yield merely decreased from ~30% to ~27% during 100 h of TOS.

To clarify the role of external surface in the alkylation of benzene with ethylene, 2,4-dimethylquinoline (2,4-DMQ) with too large molecular dimension to enter into the 10-MR pores of MWW zeolites was employed to poison selectively the acid sites on the external surface [44]. When the reactions were carried out in the absence of 2,4-DMQ, the EBs yield was 24% and 30% for H-MCM-22 and H-MCM-56 prepared from the same precursor (Si/Al = 15), respectively (Fig. 8). When the 2,4-DMQ was co-fed with benzene into the reactor, the alkylation was essentially retarded, giving extremely low EBs yields. In the case of esterification of acetic acid with ethanol, that is, a reaction involving only small molecules, H-MCM-22 was even slightly more active than H-MCM-56 (see Fig. S6 in Supplementary information). Furthermore, the addition of 2,4-DMQ into the reactants had no obvious influence on the conversion of acetic acid for both catalysts. Above results indicated that 2,4-DMQ may poison selectively the acid sites on the external surface but not those located in the 10-MR channels. The benzene ethylation that involves bulky molecules in both reactants and products is assumed to be catalyzed by the acid sites existing in open reaction spaces, those located in the 12-MR side pockets (or half cups) on the external surface of the MWW layers in case of MCM-22 [15]. Possessing a partially delaminated structure and characteristic of larger external surface, MCM-56 analogue

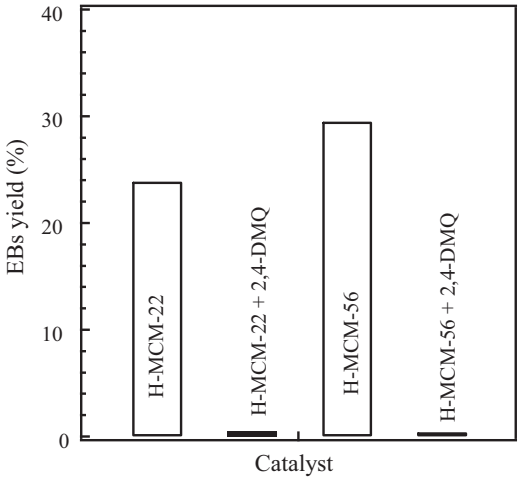

Fig. 8. Effect of 2,4-DMQ addition on the alkylation of benzene with ethylene on H-MCM-22 and H-MCM-56. Reaction conditions: catalyst, 1.0 g; temperature, 463 K; pressure, 3.0 MPa; benzene/ethylene molar ratio, 3.0; ethylene WHSV, 1.0 h^{-1}; 2,4-DMQ feed (if added), 50 μL h^{-1}; benzene feed, 19.2 mL h^{-1}; TOS = 20 h.

is benefit to the bulky reactions such as benzene ethylation. The larger external surface would be also effective for suppressing the catalyst deactivation by coke formation.

4. Conclusions

MCM-56 analogues with various Al contents have been post-synthesized from fully crystallized MCM-22 precursors by a mild acid treatment. A partial removal of interlayer organic species in the precursors probably induces a disordered collection and stacking of MWW layers, leading to a large portion of external surface exposed to the outside and partially delaminated structure of MCM-56 analogues. This endows MCM-56 catalysts with higher accessibility to bulky reactant molecules and then higher yields of ethylated benzenes as well as catalytic stability than conventional MCM-22 catalyst in the liquid-phase alkylation of benzene with ethylene.

Acknowledgements

We gratefully acknowledge the NSFC of China (220925310 and U1162102), the Shanghai Municipal Education Commission

(11CXY20), Ministry of Science and Technology (2012BAE05B02), and the Shanghai Leading Academic Discipline Project (B409) for financial support.

Appendix A. Supplementary data

Supplementary data associated with this article can be found, in the online version, at http://dx.doi.org/10.1016/j.apcata.2012.07.028.

References

[1] V.R. Vijayaraghavan, K.J.A. Raj, J. Mol. Catal. A: Chem. 207 (2004) 41–50.
[2] K.J.A. Raj, E.J.P. Malar, V.R. Vijayaraghavan, J. Mol. Catal. A: Chem. 243 (2006) 99–105.
[3] B. Yilmaz, U. Müller, Top. Catal. 52 (2009) 888–895.
[4] W.P. Addiego, W. Liu, T. Boger, Catal. Today 69 (2001) 25–31.
[5] T.F. Degnan Jr., C.M. Smith, C.R. Venkat, Appl. Catal. A: Gen. 221 (2001) 283–294.
[6] M. Lenarda, L. Storaro, G. Pellegrini, L. Piovesan, R. Ganzerla, J. Mol. Catal. A: Chem. 145 (1999) 237–244.
[7] C. Perego, P. Ingallina, Catal. Today 73 (2002) 3–22.
[8] C. Martínez, A. Corma, Coord. Chem. Rev. 255 (2011) 1558–1580.
[9] A. Corma, Chem. Rev. 95 (1995) 559–614.
[10] N.Y. Chen, W.E. Garwood, Catal. Rev. Sci. Eng. 28 (1986) 185–264.
[11] J. Cejka, A. Vondrová, B. Wichterlová, G. Vorbeck, R. Fricke, Zeolites 14 (1994) 147–153.
[12] W. Vermeiren, J.P. Gilson, Top. Catal. 52 (2009) 1131–1161.
[13] G. Bellussi, G. Pazzuconi, C. Perego, G. Girotti, G. Terzoni, J. Catal. 157 (1995) 227–234.
[14] Y.C. Du, H. Wang, S. Chen, J. Mol. Catal. A: Chem. 179 (2002) 253–261.
[15] A. Corma, V. Martínez-Soria, E. Schnoeveld, J. Catal. 192 (2000) 163–173.
[16] P. Chu, M.E. Landis, Q.N. Le, US Patent 5 334 795 (1994) to Mobil Oil Corp.
[17] J. Cheng, T. Degnan, J. Beck, Y. Huang, M. Kalyanaraman, J. Kowalski, C. Loehr, D. Mazzone, Stud. Surf. Sci. Catal. 121 (1999) 53–60.
[18] M.E. Leonowicz, J.A. Lawton, S.L. Lawton, M.K. Rubin, Science 264 (1994) 1910–1913.
[19] K.J. Del Rossi, A. Huss Jr., US Patent 5 107 047 (1992) to Mobil Oil Corp.
[20] S.I. Zones, D.I. Holtermann, R.A. Innes, T.A. Pecoraro, D.S. Santilli, J.N. Ziemer, US Patent 4 826 667 (1989) to Chevron Research Company.
[21] L. Puppe, J. Weisser, US Patent 4 439 409 (1984) to Bayer Aktiengesellschaft.
[22] M.A. Camblor, A. Corma, M.J. Díaz-Cabañas, Ch. Baerlocher, J. Phys. Chem. B 102 (1998) 44–51.
[23] S.L. Lawton, A.S. Fung, G.J. Kennedy, L.B. Alemany, C.D. Chang, G.H. Hatzikos, D.N. Lissy, M.K. Rubin, H.K.C. Timken, S. Stenernagel, D.E. Woessner, J. Phys. Chem. 100 (1996) 3788–3798.
[24] A.S. Fung, S.L. Lawton, J. Roth, US Patent 5 362 697 (1994) to Mobil Oil Corp.
[25] G.G. Juttu, R.F. Lobo, Micropor. Mesopor. Mater. 40 (2000) 9–23.
[26] L. Wang, Y. Liu, Y. Wang, W. Xie, M. He, P. Wu, Stud. Surf. Sci. Catal. 174 (2008) 241–244.
[27] Y. Wang, Y. Liu, L. Wang, H. Wu, X. Li, M. He, P. Wu, J. Phys. Chem. C 113 (2009) 18753–18760.
[28] A. Corma, U. Diaz, V. Fornés, J.M. Guil, J. Martínez-Triguero, E.J. Creyghton, J. Catal. 191 (2000) 218–224.
[29] L. Wang, Y. Wang, Y. Liu, L. Chen, S. Cheng, G. Gao, M. He, P. Wu, Micropor. Mesopor. Mater. 113 (2008) 435–444.
[30] W.J. Roth, Stud. Surf. Sci. Catal. 158 (2005) 19–26.
[31] W.D. Harkins, G.J. Jura, J. Chem. Phys. 11 (1943) 431–432.
[32] G.J. Kennedy, S.L. Lawton, M.K. Rubin, J. Am. Chem. Soc. 116 (1994) 11000–11003.
[33] M. Hunger, S. Ernst, J. Weitkamp, Zeolites 15 (1995) 188–192.
[34] M.A. Camblor, C. Corell, A. Corma, M.J. Díaz-Cabañas, S. Nicolopoulos, J.M. González-Calbet, M. Vallet-Regí, Chem. Mater. 8 (1996) 2415–2417.
[35] W. Kolodziejski, C. Zicovich-Wilson, C. Corell, J. Pérez-Pariente, A. Corma, J. Phys. Chem. 99 (1995) 7002–7008.
[36] P. Wu, T. Komatsu, T. Yashima, Micropor. Mesopor. Mater. 22 (1998) 343–356.
[37] X. Sun, L. Wang, L. Xu, S. Liu, Catal. Lett. 94 (2004) 75–79.
[38] K. Okumura, M. Hashimoto, T. Mimura, M. Niwa, J. Catal. 206 (2002) 23–28.
[39] T.F. Degnan, A.S. Fung, T.E. Helton, S.L. Lawton, D.N. Lissy, W.J. Roth, US Patent 5 536 894 (1996) to Mobil Oil Corp.
[40] A.W. Chester, A.S. Fung, C.T. Kresge, W.J. Roth, US Patent 5 779 882 (1998) to Mobil Oil Corp.
[41] A. Corma, M. Diazcabanas, M. Moliner, C. Martinez, J. Catal. 241 (2006) 312–318.
[42] J.P. Lange, A. Gutsze, J. Allgeier, H.G. Karge, Appl. Catal. 45 (1988) 345–356.
[43] S. Laforge, D. Martin, J.L. Paillaud, M. Guisnet, J. Catal. 220 (2003) 92–103.
[44] S. Namba, S. Nakanishi, T. Yashima, J. Catal. 88 (1984) 505–508.